IOP Publishing Phys. Med. Biol. 64 (2019) 245013 (15pp) https://doi.org/10.1088/1361-6560/ab5b6c

Physics in Medicine & Biology

IPEM Institute of Physics and Engineering in Medicine

OPEN ACCESS

PAPER

Standardised quantitative radioiodine SPECT/CT Imaging for multicentre dosimetry trials in molecular radiotherapy

Rebecca A Gregory[1], Iain Murray[2], Jonathan Gear[2], Francesca Leek[2], Sarah Chittenden[2], Andrew Fenwick[3], Jill Wevrett[3,4,5], James Scuffham[4,5], Jill Tipping[6], Brian Murby[6], Steve Jeans[6], Martha Stuffins[4,5], Sofia Michopoulou[7], Matthew Guy[7], Darren Morgan[8], Aida Hallam[8], David Hall[9], Heather Polydor[9], Colin Brown[10], Gerry Gillen[10], Nathan Dickson[11], Sarah Brown[12], Jonathan Wadsley[13] and Glenn Flux[2]

[1] Barts Health NHS Trust, London, United Kingdom
[2] The Royal Marsden NHS Foundation Trust and Institute of Cancer Research, Sutton, United Kingdom
[3] National Physical Laboratory, Teddington, United Kingdom
[4] Royal Surrey County Hospital NHS Foundation Trust, Guildford, United Kingdom
[5] University of Surrey, Guildford, United Kingdom
[6] The Christie NHS Foundation Trust, Manchester, United Kingdom
[7] University Hospital Southampton NHS Foundation Trust, Southampton, United Kingdom
[8] Oxford University Hospitals NHS Foundation Trust, Oxford, United Kingdom
[9] University Hospitals Bristol NHS Foundation Trust, Bristol, United Kingdom
[10] Gartnavel General Hospital, Glasgow, United Kingdom
[11] Nottingham Universities Hospitals NHS Trust, Nottingham, United Kingdom
[12] University of Leeds, Leeds, United Kingdom
[13] Weston Park Hospital, Sheffield, United Kingdom

E-mail: rebecca.gregory11@nhs.net

RECEIVED
18 August 2019

REVISED
31 October 2019

ACCEPTED FOR PUBLICATION
25 November 2019

PUBLISHED
19 December 2019

Keywords: molecular radiotherapy, radioiodine, dosimetry

Supplementary material for this article is available online

Abstract

The SEL-I-METRY trial (EudraCT No 2015-002269-47) is the first multicentre trial to investigate the role of ^{123}I and ^{131}I SPECT/CT-based tumour dosimetry to predict response to radioiodine therapy. Standardised dosimetry methodology is essential to provide a robust evidence-base for absorbed dose–response thresholds for molecular radiotherapy (MRT). In this paper a practical standardised protocol is used to establish the first network of centres with consistent methods of radioiodine activity quantification.

Nine SPECT/CT systems at eight centres were set-up for quantitative radioiodine imaging. The dead-time of the systems was characterised for up to 2.8 GBq ^{131}I. Volume dependent calibration factors were measured on centrally reconstructed images of ^{123}I and ^{131}I in six (0.8–196 ml) cylinders. Validation of image quantification using these calibration factors was performed on three systems, by imaging a 3D-printed phantom mimicking a patient's activity distribution. The percentage differences between the activities measured in the SPECT/CT image and those measured by the radionuclide calibrator were calculated. Additionally uncertainties on the SPECT/CT-based activities were calculated to indicate the limit on the quantitative accuracy of this method.

For systems set-up to image high ^{131}I count rates, the count rate versus activity did not peak below 2.8 GBq and fit a non-paralysable model. The dead-times and volume-dependent calibration factors were comparable between systems of the same model and crystal thickness. Therefore a global calibration curve could be fitted to each. The errors on the validation phantom activities' were comparable to the measurement uncertainties derived from uncertainty analysis, at 10% and 16% on average for ^{123}I and ^{131}I respectively in a 5 cm sphere.

In conclusion, the dead-time and calibration factors varied between centres, with different models of system. However, global calibration factors may be applied to the same system model with the same crystal thickness, to simplify set-up of future multi-centre MRT studies.

1. Introduction

Currently there is little evidence to guide the optimum activity of radioiodine to be delivered in the management of differentiated thyroid cancer (DTC) (Luster *et al* 2008, Silberstein *et al* 2012, Dietlein *et al* 2016). Therefore treatment methods vary widely between centres. In the majority of cases fixed activities are administered rather than individualised prescriptions according to the radiation doses delivered to target volumes or normal tissues. The EU Directive concerned with basic safety standards for protection against the dangers arising from exposure to ionising radiation, requires that radiation therapies should be individually planned (2013/59/Euratom 2014).

Absorbed dose–response thresholds need to be identified to prescribe radiation doses for treatment planning. The European Association of Nuclear Medicine Therapy Committee guidelines quote thresholds derived in 1992 on now out-dated planar imaging equipment for patients at a single centre (Maxon *et al* 1992, Luster *et al* 2008). Modern SPECT/CT systems are becoming more widely available and are gaining acceptance as an accurate quantitative imaging modality (Bailey *et al* 2014). Iodine-131 SPECT/CT imaging with attenuation and scatter compensation has been shown to achieve quantitative accuracy within 5%–15% (Dewaraja *et al* 2013). Further studies are required to collect data to establish absorbed dose thresholds and good standards of practice for individualised molecular radiotherapy (MRT) planning. Currently MRT treatments are relatively infrequent compared to other modalities of radiation therapy. Multicentre trials incorporating dosimetry, such as the SEL-I-METRY trial (EudraCT No 2015-002269-47), are therefore essential (McGowan *et al* 2015, NCRI 2016, Giammarile 2018, Brown *et al* 2019).

The measurements described in the paper were performed to provide robust dosimetry results obtained from the SEL-I-METRY trial. This is the first multicentre phase II MRT trial with an exploratory endpoint to investigate the role of dosimetry to predict response to radioiodine therapy. The primary objective of this study is to investigate the potential of Selumetinib (AZD6244, ARRY-142886) to re-sensitise advanced iodine-refractory DTC (IR-DTC) to recombinant thyroid stimulation hormone (rhTSH) stimulated radioiodine uptake (Wadsley *et al* 2017). In a pilot study performed at Memorial Sloan-Kettering Cancer Centre, 20 patients with IR-DTC underwent a ^{124}I PET/CT scan before and after 28 d of treatment with 75 mg Selumetinib. Radioiodine therapy was given to these patients if, based on the single PET/CT scan, one or more lesions were predicted to receive greater than an arbitrary absorbed dose of 20 Gy for therapeutic ^{131}I activities up to 11.1 GBq. This treatment schedule was successful in 8 of those patients, resulting in subsequent evidence of radiological response or disease stabilisation, but the absorbed dose-response correlation has not been published (Ho *et al* 2013). The SEL-I-METRY trial aims to replicate these findings for a larger cohort of 60 patients in a multicentre trial. The ability of Selumetinib to enhance radioiodine uptake will be assessed from ^{123}I planar whole body and SPECT/CT scans acquired at baseline and following the 28 d course of Selumetinib. Patients showing evidence of new sites of iodine uptake or 30% increased iodine uptake in existing iodine avid lesions will undergo a further 2–3 ^{123}I SPECT/CT scans acquired up to 72 h following administration. The activities measured from these images will be used to produce time-activity curves for absorbed dose calculations to predict the therapeutic ^{131}I absorbed dose. In the absence of an established absorbed dose response threshold for DTC metastases, all patients will receive ^{131}I therapy at a fixed activity of 5.5 GBq. Dosimetry will then be performed from 3 to 4 SPECT/CT scans acquired up to 144 h following ^{131}I administration. This will be compared to the predicted absorbed doses and will be correlated with the patient's treatment response in order to establish absorbed dose response thresholds for this treatment (Wadsley *et al* 2017).

Absorbed dose estimates are dependent on the measurement methods used and the corrections made to those measurements to quantify the *in vivo* radioactivity. For example in 1983 Maxon established a 300 Gy threshold required to ablate the thyroid remnants, using activities measured on a rectilinear scanner (Maxon *et al* 1983). This was higher than the value identified through SPECT measurements at 49 Gy in 2010 (Flux *et al* 2010) and 90 Gy through ^{124}I PET measurements (Wierts *et al* 2016). Additionally an 85 Gy threshold was established for successful treatment of metastatic disease using the rectilinear scanner (Maxon *et al* 1992). However more recent ^{124}I PET measurements indicated a lower threshold at 40 Gy (Wierts *et al* 2016). The accuracy of scintigraphic image quantification has been shown to vary widely between centres unless a harmonised calibration and image analysis protocol is adopted (Zimmerman *et al* 2017). Therefore it is clear that standardisation of dosimetry methodology is an essential component of any multi-centre trial aiming to provide a robust evidence-base for absorbed dose–response thresholds. Consequently a network of centres providing treatment, performing standardised quantitative imaging and dosimetry calculations has been established for the SEL-I-METRY trial. The aim of this paper is to describe the standardised SPECT/CT calibration methodology used in this trial, as well as to present the results of validation measurements performed to assess the accuracy of the multi-centre methodology. Protocols were developed with the aim of providing quantitative accuracy whilst making the best possible use of the technology available at all sites. The results from implementing these across seven participating centres are also given.

Table 1. Centres' SPECT/CT systems.

Centre	SPECT/CT system		Field-of-view (mm)	NaI thickness (mm)
A	Siemens	Symbia (Intevo Excel) I1	614	9.5
		Symbia (Intevo Excel) I2	614	9.5
B		Symbia (Intevo Excel)	614	9.5
C		Symbia (T2)	614	9.5
D		Symbia (T16)	614	15.9
E	GE	600 Series (Optima 640)	565	9.5
F		600 Series (Discovery 670) 1	540	9.5
G		600 Series (Discovery 670) 2	540	9.5
H		600 Series (Discovery 670) 3	540	9.5

Table 2. Collimator specifications.

Camera	Collimator	Hole diameter (mm)	Septal thickness (mm)	Length (mm)
Siemens	MELP[a]	2.94	1.14	40.6
	HEGP	4.0	2.0	59.7
GE	MEGP	3.0	1.05	58.0
	HEGP	4.0	1.80	66.0

[a] MELP = medium-energy low penetration, Siemens' equivalent of MEGP = medium-energy general-purpose. HEGP = High-energy general-purpose.

2. Methods

The eight centres participating in the trial were equipped with a total of four different models of SPECT/CT camera systems, described in table 1. The basic designs of the gamma cameras were very similar. The main differences were the collimator specifications and methods for handling dead-time. Additionally, one centre (D) had a thicker NaI crystal than the other sites.

Medium-energy general-purpose (MEGP) collimators have previously been shown to be the most suitable for quantitative ^{123}I imaging (Gregory *et al* 2017). High-energy general-purpose (HEGP) collimators have been shown to be most suitable for imaging ^{131}I (Dewaraja *et al* 2013). Collimator specifications for each manufacturer are summarised in table 2.

All of the centres used Capintec CRC 15R dose calibrators to assay ^{131}I and ^{123}I. These calibrators all had calibrations traceable to the UK's National Physical Laboratory (NPL) primary standard. A copper filter was used for ^{123}I measurements.

Prior to site set up the sites were asked to perform intrinsic uniformity tests with ^{99m}Tc, ^{123}I and ^{131}I, centre-of-rotation and SPECT/CT alignment checks, and MEGP and HEGP extrinsic uniformity tests on the SPECT/CT systems. Sites were also required to perform quality control of their weighing scales and radionuclide calibrators. Local protocols were followed at each site for these tests. Sites were asked to ensure the radioiodine intrinsic integral and differential central field of view (FOV) uniformity were within 4% and 3% respectively and to visually inspect the images to ensure there were no major tube artefacts.

A standardised SPECT acquisition protocol was developed in collaboration with physicists from each of the sites (table 3). The acquisition protocols currently used at the Royal Marsden Hospital were used as a starting point for discussions (Flux *et al* 2010). These were adapted to create a practical standardised protocol, whilst making the best possible use of the technology available at all sites.

As the patients' count rates in this study may be very low at late time-points, the number of projection angles was set to 72 to allow each projection to be collected for a longer time to limit image noise, whilst maintaining a tolerable imaging time for the patient. The matrix size was set at 128 × 128. Additionally the photo-peak energy windows were set to a width of 20%. Further 6% wide energy windows were set adjacent to the peak energy window, to allow scatter correction using a triple energy window correction (TEWC) (van Gils *et al* 2016).

2.1. SPECT/CT system calibration

The SPECT/CT images were corrected for count losses due to dead-time, resolution and partial volume effects (PVE) using calibration factors acquired for different detected count rates and object volumes. The object activity concentrations α_{meas} were then calculated as

Table 3. Standardised acquisition protocol.

Radioisotope	^{123}I	^{131}I
Collimator	MEGP/LP	HEGP
Peak energy window (EW)	159 keV ± 10%	364 keV ± 10%
Low scatter EW	138 keV ± 3%	318 keV ± 3%
High scatter EW	180 keV ± 3%	413 keV ± 3%
Matrix	128 × 128	
SPECT movement	Body contour	
Projections	72 (5°/projection)	

$$\alpha_{meas} = \frac{D_\tau C}{dQ}. \quad (1)$$

Where D_τ is the measured system dead time, C is the mean count measured in a volume of interest (VOI) defined about the object on the SPECT/CT image, d is the duration of the scan and Q is the volume specific calibration factor.

These factors are dependent on the acquisition and reconstruction protocol and were therefore made for the standardised acquisition protocol (table 3). The systems were calibrated in a standardised way to provide comparable quantitative accuracy between the systems.

2.1.1. *Dead-time characterisation*

Dead-time was characterised on the nine systems following the protocol given in supplementary information A (stacks.iop.org/PMB/64/245013/mmedia). A brief description of these measurements follows.

The 6.5 l cylindrical Jaszczak phantom was filled with water and 1 g of Potassium Iodide and 1 g Sodium Thiosulphate were added to prevent the radioiodine from binding to the phantom walls. An air gap of approximately 2 cm was left at the top of the phantom to allow solution mixing. The phantom was positioned with its flat base on the couch and the detector surfaces were positioned as close to the phantom flat base and lid as possible (figure 1). A 10 min background static scan was acquired. ^{131}I was then added incrementally to the phantom, agitating the phantom liquid each time to uniformly distribute the activity. A 100 kcount static scan was acquired at each activity level. In total fifteen activity levels were scanned, ranging from 20 MBq to 2.8 GBq. For a 5.5 GBq therapy administration, this was assumed to be the highest activity that will be likely to be seen in a trial patient 24 h after administration.

The count rate in the photo-peak energy window for each detector at each activity was recorded. The true count rates R_T at higher activities were extrapolated linearly from the first five measured counts rates R_M at activities below 100 MBq. These were assumed to be free from dead-time induced count losses. The equations for the paralysable system

$$R_M = R_T e^{-R_T \tau}, \quad (2)$$

and non-paralysable systems

$$R_T = \frac{R_M}{(1 - R_M \tau)}, \quad (3)$$

were fitted to the count rates to determine the resolving time τ, using Graphpad Prism analysis software (v6.07) (Dewaraja 2013). The dead time correction factor D_τ for the non-paralysable model is then R_T/R_M.

The dead-time characterisation at centre E initially showed that the standard GE detection mode peak count rates were paralysable and reached a maximum count rate for 1.6 GBq. Count rates at higher activities were indistinguishable from those resulting from lower activities, preventing calibration of the system above 1.6 GBq (figure 5). The 'Fast' mode for ^{131}I on each of the GE systems within this study network was therefore optimised by the manufacturer to reduce the dead-time at high count rates. The system at centre E was tested with and without 'Fast' mode, and all subsequent GE systems were prepared with 'Fast' mode by the manufacturer before carrying out the SEL-I-METRY calibrations. The design of the Siemens SPECT/CT cameras, tested in this study, did not require the user to switch modes specifically to image at high count rates: switching occurs automatically.

2.1.2. *Volume dependent calibration*

Nine SPECT/CT systems were calibrated incorporating PVE correction following the protocol in the supplementary information B. A brief description of the measurements follows.

Six cylinders were imaged, positioned 8 cm from the central axis of a torso shaped phantom filled with inactive water, shown in figure 2. The cylinders ranged from 1.0 to 6.2 cm in diameter and length and their volumes

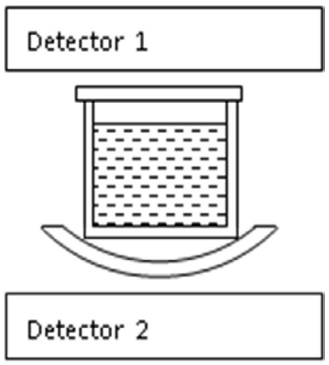

Figure 1. Cylindrical phantom positioning.

ranged from 0.8 to 196 ml. The diameter and length of each was the same, these are marked next to the cylinders in figure 2. These were filled with 0.24 ± 0.04 MBq ml^{-1} of first ^{123}I, then subsequently ^{131}I in a separate set of measurements. The radioiodine was suspended in a Potassium Iodide and Sodium Thiosulphate solution. The total activity of the phantom for each measurement was approximately 100 MBq to avoid dead-time effects in the ^{131}I measurements.

SPECT scans were acquired with the standard acquisition protocol for the appropriate isotope (table 3), at 60 s per projection. A CT scan was acquired for attenuation correction (AC), using each site's standard low-dose protocol.

All SPECT images were reconstructed centrally at Site A using HERMES Hybrid Recon (Hermes Medical Solutions, Stockholm, Sweden) reconstruction software. The CT scan was converted to an attenuation map and used for AC. Ordered-subsets expectation maximisation (OSEM) reconstruction with eight iterations and four subsets was performed on all the data sets with Monte Carlo Scatter Correction (Sohlberg *et al* 2012). The number of iterations was chosen based on qualitative assessment of the first patient's dosimetry scans to achieve an image with a noise level that was practical for lesion identification and therefore VOI definition. The ^{123}I images were additionally smoothed using the maximum *a posteriori* (MAP) algorithm with a smoothing prior (MAPsmoothing) β-value of 0.6 to reconstruct the images (Green 1990).

Volumes of interest were defined manually about the physical boundary of the cylindrical inserts on the CT images. These CT-based VOIs were copied to the SPECT images and in doing so the VOI voxels were resampled to match the SPECT voxel size. The mean voxel count rates in the VOIs R_{Cyl} were divided by the known average decay corrected activity concentration, α, over the time length of the scan, measured at filling.

$$\alpha = \alpha_0 e^{\left(-\frac{\ln(2)(t_m - t_0)}{t_{\frac{1}{2}}}\right)} \tag{4}$$

where α_0 is the activity concentration at the start of the scan, t_0 is the time at the start of the scan, $t_{1/2}$ is the radioiodine half-life and t_m is the mid-time of the scan given by

$$t_m = t_0 + \ln\left[\frac{d}{(1 - e^{-d})}\right] \tag{5}$$

where λ is the decay factor $\ln 2/t_{1/2}$ and d is the duration of the scan. Therefore the volume specific calibration factor, Q (cps/MBq/ml), for each cylinder volume is

$$Q = \frac{R_{Cyl}}{\alpha_{Cyl}}. \tag{6}$$

These factors were plotted against the cylinder volume to provide recovery curves (Hoffman *et al* 1979).

A VOI was also defined about the CT image of the outer torso-shaped phantom. The total count rate R_{Tot} in the VOI was assumed to originate from the total volume of the active cylinders, V_C. Therefore R_{Tot}/V_C was assumed to be the mean count rate per unit volume that would be observed in the absence of PVE. The activity concentration, α_{Cyl}, was divided by this mean count rate to provide a calibration factor in the absence of PVE, q. This is the equivalent of the system sensitivity (voxel MBq/ml/cps) for that activity distribution and attenuating media. The error on this value was calculated from propagation of the errors in the activity concentration and count, as described in section 2.3.

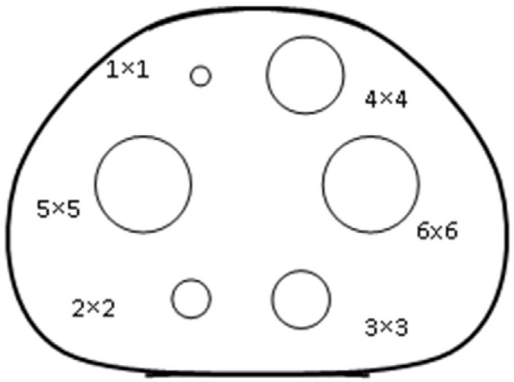

Figure 2. A schematic drawing of the volume dependent calibration phantom cross-section, showing the dimensions (cm) and positions of each of the cylinders.

Graphpad Prism (6.07) was used to fit the following equation to the measured factors.

$$Q = \frac{q}{\left(1 + (\gamma/v)^{\beta}\right)}. \tag{7}$$

Where v is the cylinder volume and β and γ are the fit parameters. The plateau of this curve was constrained to the factor in the absence of PVE, q, defined above. The covariance and standard errors associated with the fit parameters β and γ were used in the uncertainty estimation calculations at validation (section 2.3).

2.2. Staff radiation dose assessment

Where available, operators handling radiation for these calibrations wore electronic personal dosimeter (EPDs) at waist height. The tasks involving radioactive source handling were typically shared between 2 to 4 staff members to reduce the dose received by any one member of staff. All operators were experienced in handling unsealed sources and adopted good radiation protection practice to maintain their distance from the radiation sources whenever possible, limit the time they handled the sources and to use the available shielding. The mean staff EPD dose was calculated.

2.3. Validation—assessment of quantitative accuracy

A further set of experiments were performed to validate the accuracy of the calibration procedures. 3D printed inserts were manufactured to mimic the challenge of clinical imaging. Phantom inserts were designed based on the images of the first patient that received ^{131}I treatment and further dosimetry scans. This patient was imaged according to the SEL-I-METRY trial protocol (Wadsley *et al* 2017, Brown *et al* 2019).

The largest lesion, a 60 ml sub-carinal node, was outlined on the CT image using Hermes software, as shown in figure 3. Where the border of the lesion was unclear the SPECT image was used to guide outlining. This outline was uploaded into Autodesk® MeshMixer software to design a 3D printed fillable phantom insert. A filling tube was added to the design that additionally acted as a support stem for the insert to be attached to a specially adapted lid for the IEC phantoms. Three of these identically shaped lesion inserts were designed with 20, 38 and 61 ml volumes, excluding the filling tube. The filling tube length positioned the centre of each lesion 7 cm away from the lid. These objects were printed on an Objet-Eden 350 3D printer with Stratasys clear bio-compatible (Med610) printing material (Gear *et al* 2014).

In order to achieve a realistic scan the activity used to fill the lesion-shaped inserts was chosen to be as similar as possible to that measured in the patient at the 24 h scan. In order to account for patient motion between the CT and SPECT acquisition, a threshold VOI was defined on the SPECT image for radioiodine quantification. The threshold was adjusted iteratively until the SPECT defined VOI volume matched the CT volume. Using this approach the ^{131}I activity in the patient's lesion was estimated to be 290 MBq at 24 h. Therefore for validation of the ^{131}I SPECT images, the inserts were filled with 916 MBq (4.730 $\pm$ 0.079 MBq ml^{-1}) ^{131}I. The activity of the largest lesion-shaped insert was 293 $\pm$ 5 MBq, corresponding to 6.5% uptake of the 5.5 GBq therapeutic radioiodine. Therefore the equivalent largest lesion activity for validation of the ^{123}I SPECT images was calculated as 6.5% of the administered 370 MBq ^{123}I, decay corrected to 24 h and the inserts were filled with 0.122 $\pm$ 0.007 MBq ml^{-1} ^{123}I, so that the largest lesion was filled with 6.8 $\pm$ 0.4 MBq.

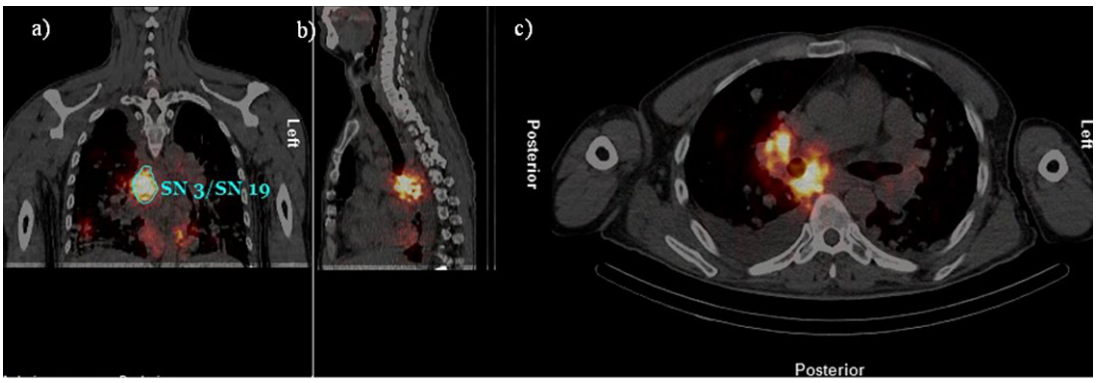

Figure 3. (a) Coronal, (b) sagittal and (c) transverse slices of the ^{123}I SPECT/CT image of the first patient, showing the outline of the sub-carinal node.

The lesions were positioned within the phantom as shown in figure 4. The background of a cylindrical phantom was filled with inactive water and polystyrene beads to mimic the attenuation of lungs. This phantom was placed in the abdomen shaped IEC phantom shell. This outer shell was filled with inactive water. Figure 4 shows a cross-sectional diagram of the filled phantom. This phantom was scanned on 3 of the systems within the network; the Siemens Intevo systems located at site A and the GE system at site E. The phantom was scanned with the lesion-shaped inserts filled with ^{123}I and rescanned with the inserts filled with ^{131}I, at the activity concentrations described above.

During scanning, the IEC phantom containing the lesion-shaped inserts was positioned on the couch with its central axis aligned as close as possible to the CT scanner central axis. The phantom scan was acquired for 60 s per projection for the ^{123}I scan to match the image acquisition for the patient. The ^{131}I SPECT/CT scan was performed using the study patient imaging protocol using 5 s per projection to match the scan duration used for the patient. The images were reconstructed using the trial reconstruction protocol (described in section 2.1.2).

The total acquired scan count rate R_M was used to calculate the dead time, D_T, for the ^{131}I images using equation (3). Each VOI volume was used to determine the volume specific calibration factor, Q. The activity in the SPECT image α was calculated using equation (1).

The percentage difference ($\%D$) between the SPECT/CT-measured activity concentrations, and those measured using the calibrator, a_{Cal}, was used to evaluate the quantitative accuracy,

$$\%D = 100 \times \frac{(\alpha - a_{Cal})}{a_{Cal}}. \tag{8}$$

2.3.1. *Uncertainty analysis*

Uncertainty analysis was performed according to EANM guidelines regarding the assessment of error propagation in dosimetry (Gear *et al* 2018). As the volume was determined on the CT, the uncertainty on the object's volume v that could be measured on the SPECT image outline was calculated from the voxel size a

$$\frac{u(v)}{v} = 3\left(\frac{\sqrt{\left(\frac{a^2}{6}\right)}}{D}\right). \tag{9}$$

Where D is the diameter of a sphere with the same volume.

The uncertainty on the volume specific calibration factor Q given in equation (6) depends on the volume uncertainty and the covariance matrix $\boldsymbol{V_b}$ determined from the least square fitting process to determine the fit parameters β and γ,

If the recovery coefficient RC, the factor required to correct the activity concentration for PVE, is extracted from equations (6) and (7),

$$RC = 1 - \frac{Q}{q} = 1 - \left(\frac{1}{\left(1 + \left(\frac{\gamma}{v}\right)^{\beta}\right)}\right), \tag{10}$$

the uncertainty on RC is

$$u^2(RC) = \boldsymbol{g_b}^{\top} \boldsymbol{V_b} \boldsymbol{g_b}. \tag{11}$$

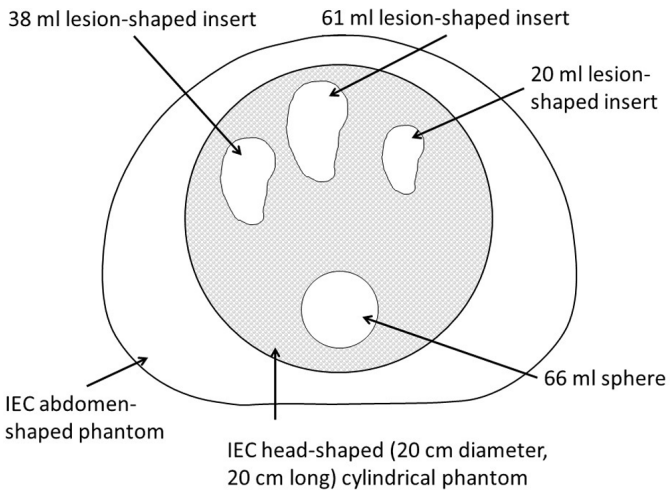

Figure 4. Cross-sectional diagram of the validation phantom. A SPECT/CT scan of this phantom is shown in figure 8.

Where $\boldsymbol{g_b}$ is a matrix containing the partial derivatives of the first order of β and γ. The uncertainty on the system sensitivity $u(q)$ was calculated as the difference ΔR_V between the count rate per unit volume R_{Tot}/v calculated on the images of the calibration cylinders and the same calculation made on the images of the validation phantom to take into account the effect of geometry on the count rate. This was combined in quadrature with the 5% error on the radionuclide calibrator activity $u(A_{cal})$ measurement based on the tolerance on the accuracy of field instruments provided by the NPL (Gadd *et al* 2007).

$$\left[\frac{u(q)}{q}\right]^2 = \left[\frac{u(A_{cal})}{A_{cal}}\right]^2 + \left[\frac{\Delta R_V}{R_V}\right]^2. \tag{12}$$

There is additional uncertainty in the measured mean counts C associated with the accuracy of the VOI definition.

$$\frac{u(C)}{C} = \frac{\varphi}{2RC}\frac{u(v)}{v} \tag{13}$$

where

$$\varphi = erf\left(\frac{2r^2}{\sigma\sqrt{2}}\right) - \frac{2\sigma}{r\sqrt{2\pi}}\left[1 - e^{-\frac{2r^2}{\sigma^2}}\right] \tag{14}$$

where r is $D/2$ and σ is the standard deviation of the Gaussian point spread function derived from the system spatial resolution, estimated as 2 mm for ^{123}I and 3 mm for ^{131}I for both systems.

$$\left[\frac{u(\widetilde{A})}{\widetilde{A}}\right]^2 = \left[\frac{u(q)}{q}\right]^2 + \left[\frac{u(RC)}{RC}\right]^2 + \left[\frac{u(C)}{C}\right]^2 - \frac{\varphi}{RC^2v}\frac{\partial RC}{\partial v}u^2(v). \tag{15}$$

The percentage difference on the activity measured in the validation image, $\%D$, was compared to the uncertainty on the measurement $u(\widetilde{A})$.

3. Results

3.1. SPECT/CT system calibration

3.1.1. Dead-time characterisation

The variation of the extrapolated versus the measured count rate on the GE systems in the standard mode is shown in figure 5(a). Above 1.6 GBq the count rates vary by less than 1 kcps as activity increases up to 2.8 GBq. Figure 5(b) shows the count rates on the GE systems after 'Fast' mode was implemented. The extrapolated versus the measured count rates are shown in figure 6, for all the characterised systems. The equations (2 and 3) for the non-paralysable and paralysable system response both fit the Siemens and GE 'Fast' mode data equally well, both with r-square values of 0.999. The resolving times for use with the non-paralysable model are given in table 4. These can be used along with equation (3) to calculate the true count rate from the measured count rate.

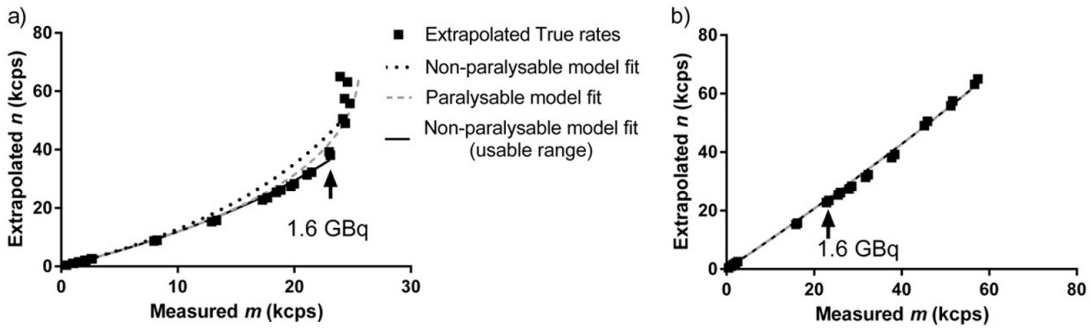

Figure 5. The extrapolated (true) versus the measured count rate for the GE systems in (a) the standard and (b) 'fast' mode.

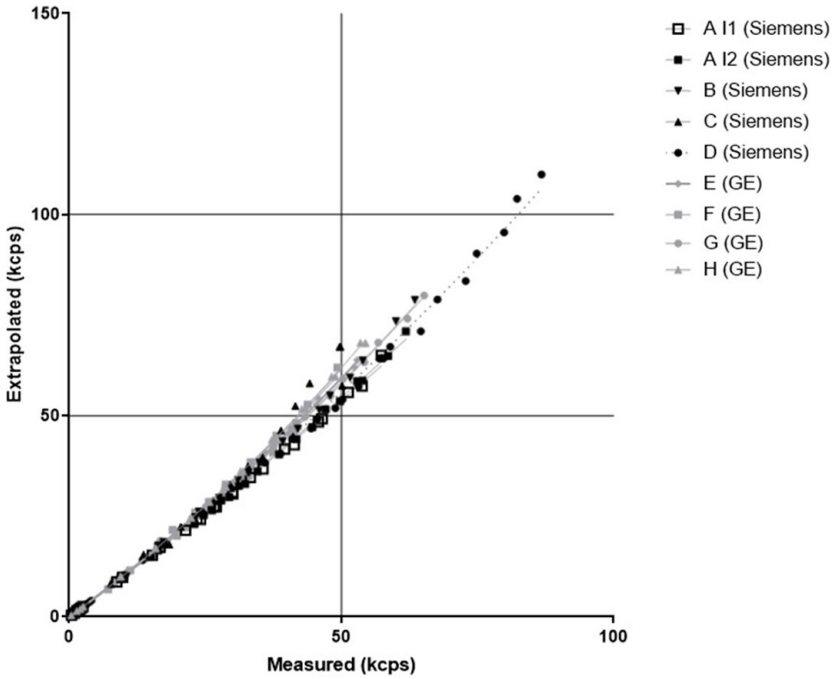

Figure 6. The extrapolated (true) versus the measured count rate for each system calibrated in this study.

3.1.2. Volume dependent calibration

The results of the calibration are shown in figure 7. The ^{123}I factors were higher on the Siemens systems.

The results in table 5 show the calibration factors for all nine systems following the standardised calibration method. These parameters may be used in equation (7) to determine calibration factors for any volume and the uncertainties on these parameters may be used for the analysis of the uncertainties in the final calculated doses. The error on q has been set to 5% to demonstrate the effect of the 5% uncertainty on the calibrator reading. The factors from the same manufacturer with the same crystal thickness were sufficiently similar that it was possible to fit shared parameters, with an r^2 value above 0.9. However the individual system parameters were used to calculate the calibration factors for the following validation and may be used for the patient data.

3.2. Staff radiation dose assessment

The mean combined whole body radiation dose to the operators was 109 ± 27 μSv shared between 2 to 4 operators at each system calibration.

3.3. Validation

Figure 8 shows SPECT/CT images of the validation phantom filled with ^{123}I. An example of the factors contributing to the uncertainty in the activity quantification of the sphere are shown in table 6 for each iodine radionuclide. Figure 9 shows the percentage of the correct activity measured in the SPECT/CT image, 100-%D calculated using equation (8), plotted for each validated centre and insert. Eighty-three per cent of validation measurements correctly estimated the activity within the estimated uncertainty. The activity concentrations

Table 4. Standardised resolving times.

Centre	Manufacturer	System	Resolving time τ [μs]
A	Siemens	Intevo (I1)	1.424 ± 0.083
		Intevo (I2)	1.691 ± 0.060
B		Intevo	2.845 ± 0.054
C		Symbia T2	3.796 ± 0.025
D		Symbia T16	2.139 ± 0.071
E	GE	Optima	3.150 ± 0.033
F		Discovery	2.796 ± 0.038
G		Discovery	1.494 ± 0.082
H		Discovery	3.864 ± 0.086

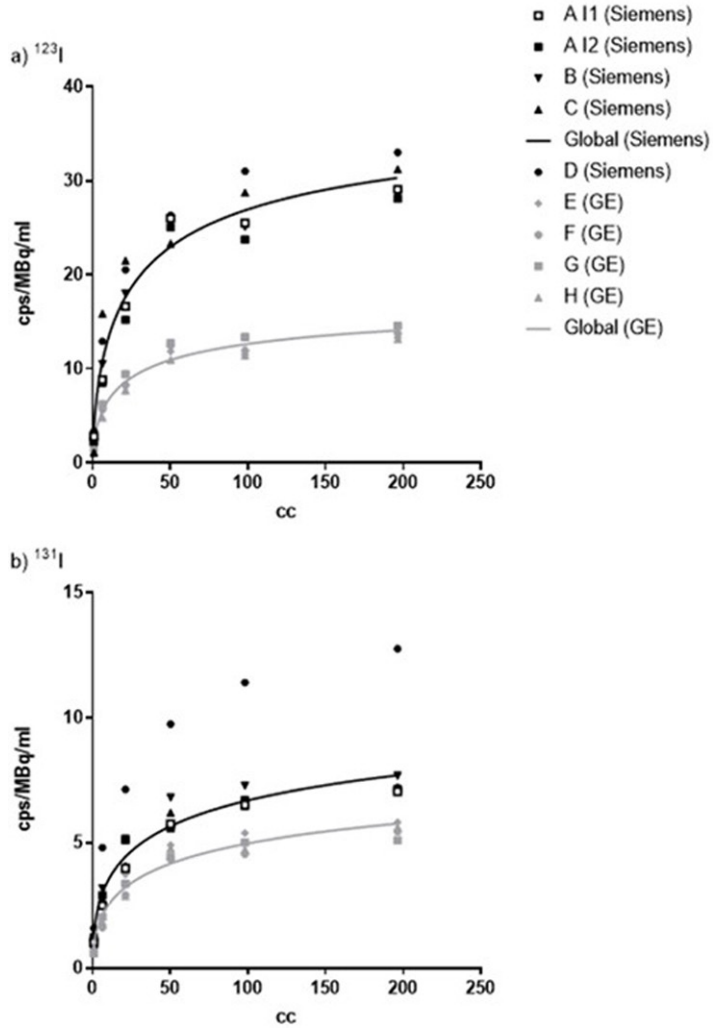

Figure 7. The PVE correction factors for (a) ^{123}I and (b) ^{131}I, along with the global curve fit to data for the same manufacturer with the same crystal thickness. The system at centre D had a thicker crystal and therefore a different calibration curve.

measured in the images differed by 10.3% and 7.1% from the activities measured at the calibrator on average for ^{131}I and ^{123}I respectively.

4. Discussion

Gamma cameras of different makes and models, across multiple sites, have been standardised for quantitative radioiodine SPECT/CT imaging to enable collation of data for multi-centre trials.. The practical standardised acquisition protocol in table 3 and the calibration protocols (supplementary data) were developed based on the findings on the technology currently available in clinical practice.

Table 5. Calibration factor Q results, for HERMES hybrid recon reconstruction with MC scatter correction.

		^{123}I			^{131}I		
		4 OSEM iterations with eight subsets, AC, MC scatter correction, no RR & MAP β 0.6			4 OSEM iterations with eight subsets, AC, MC scatter correction, no RR & no filter		
Site	System	q	γ	β	q	γ	β
A	Intevo (I1)	39.2 ± 2.0	31.3 ± 4.8	0.68 ± 0.09	12.93 ± 0.65	105.2 ± 12.1	0.480 ± 0.038
	Intevo (I2)	37.9 ± 1.9	33.1 ± 5.8	0.68 ± 0.10	13.03 ± 0.65	94.21 ± 15.1	0.425 ± 0.044
B	Intevo	38.6 ± 1.9	27.6 ± 4.4	0.63 ± 0.07	14.04 ± 0.70	85.9 ± 14.6	0.436 ± 0.050
C	Symbia T2	42.7 ± 2.1	27.0 ± 6.2	0.56 ± 0.09	12.88 ± 0.66	91.8 ± 13.8	0.480 ± 0.051
Global		39.6	29.8 ± 2.8	0.63 ± 0.05	13.22	94.01 ± 8.1	0.453 ± 0.027
D	Symbia T16[a]	43.5 ± 2.2	26.0 ± 1.5	0.63 ± 0.03	22.12 ± 1.11	91.7 ± 5.8	0.490 ± 0.022
E	Optima 640	17.3 ± 0.9	22.3 ± 3.3	0.6 ± 0.06	10.64 ± 0.53	95.0 ± 12.1	0.435 ± 0.036
F	Discovery 670	17.88 ± 0.89	23.11 ± 3.93	0.629 ± 0.080	9.901 ± 0.50	117.8 ± 15.5	0.498 ± 0.045
G	Discovery 670	20.75 ± 1.04	29.90 ± 3.23	0.541 ± 0.043	9.853 ± 0.49	71.73 ± 8.15	0.473 ± 0.038
H	Discovery 670	17.03 ± 0.87	26.33 ± 2.24	0.526 ± 0.042	9.904 ± 0.49	99.49 ± 17.4	0.500 ± 0.063
Global		18.24	25.31 ± 2.23	0.596 ± 0.035	10.07	104.6 ± 9.34	0.468 ± 0.029

[a] Thick crystal.

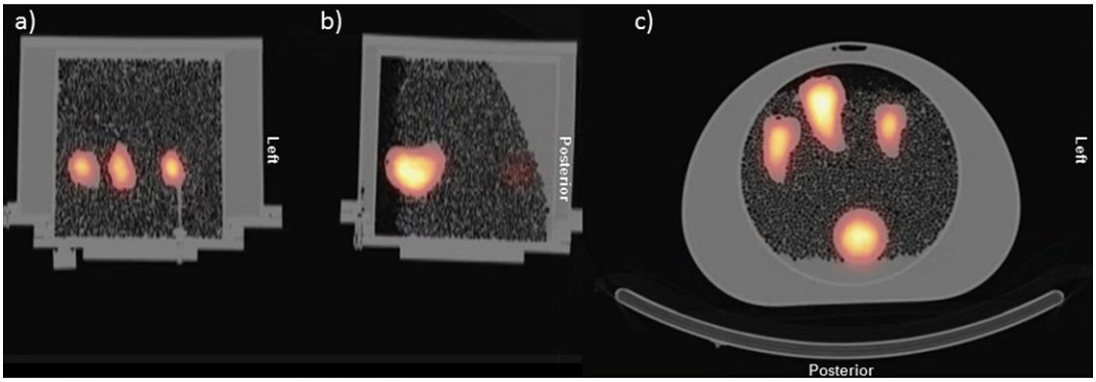

Figure 8. (a) Coronal, (b) sagittal and (c) transverse slices of the ^{123}I SPECT/CT image of the validation phantom.

Table 6. The average factors measured resulting in the activity uncertainty estimate on the 5 cm sphere.

	% uncertainty due to;			
	System sensitivity $\frac{u(q)}{q}$%	Volume dependent recovery coefficient $\frac{u(RC)}{RC}$%	VOI count $\frac{u(C)}{C}$%	% uncertainty on activity
^{123}I	5.74%	6.16%	8.57%	9.69%
^{131}I	9.27%	4.97%	11.39%	15.72%

Older gamma camera systems are known to have been prone to high dead time losses (Rosenthal *et al* 1995), preventing acquisition of dosimetry scans prior to 2 d after therapeutic radioiodine administration (Dewaraja *et al* 2013). However the characterisation of these newer systems, shown in figure 5, indicated that the GE systems operating in 'Fast' mode avoid the peak count-rate folding over at 2.4 GBq. Above 1.6 GBq (23 kcps) the count rates varied by less than 1 kcps before 'Fast' mode was implemented, and it would not be possible to quantify the images above that activity. On the Siemens system there is no specific high count-rate mode and the count-rate does not peak or reach a plateau below 2.8 GBq (70 kcps) (figure 6(c)). Therefore patients can be scanned much earlier following administration on the newer systems and the early phase of radioiodine uptake may be measured.

There are several methods available to correct dead-time. The simplest is the dual-source method to measure the resolving time. However it has been shown that for this method to be accurate the count rates from two sources needs to be within 95% of the maximum count rate of the system, requiring prior knowledge about the dead-time characteristics of the system (Silosky *et al* 2013). A reference source method provides a direct method to measure the count losses due to dead-time. However the source has to be at a low enough activity not to cause

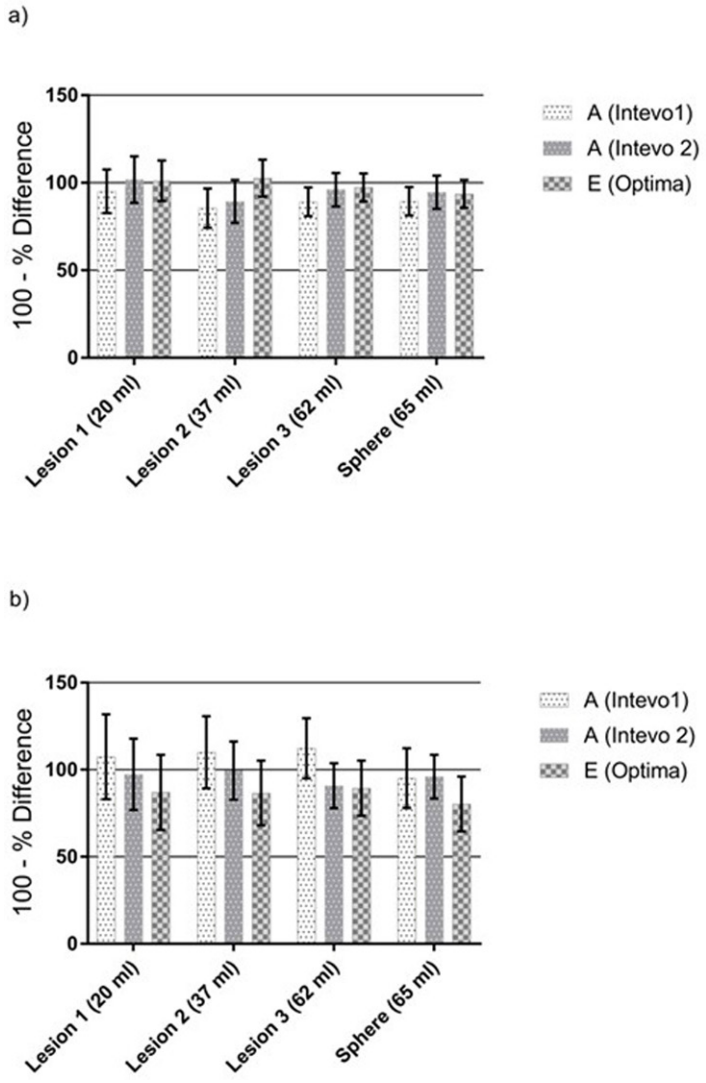

Figure 9. The difference in quantitative accuracy between the measurements obtained from the SPECT/CT and known activity concentrations, 100-%D, in (a) ^{123}I and (b) ^{131}I images, where the correct result would be 100%. The error bars were calculated from propagation of errors in the measurement process, $u(\tilde{A})$.

dead-time, so the statistical quality of the correction factor tends to be poor (Madsen *et al* 1986). Additional resources are required for each patient scan to correctly prepare and place the reference source and to acquire a scan of the reference source alone. For this reason it was not considered practical to implement these methods for a multicentre trial. Therefore a cylindrical Jaszczak phantom was scanned, which was available at all sites. Fifteen activity levels were adequate to characterise and model the dead-time. Having relatively large gaps in activity at the higher count rates kept the radiation exposure to staff reasonably low and the time required to characterise the systems to below 3 h. The phantom was stored at each site for several months following these measurements.

The average system dead-time factor at 1 GBq was 1.08. As the level of dead-time varies with the shape of the energy spectrum these factors are dependent on the object geometry and the dead-time characteristics of the gamma camera (Sorenson 1975, Inoue *et al* 1998, Siman *et al* 2015). However variation in a small correction factor for the newer systems is likely to have a less adverse effect on the quantitative accuracy than a variation in a larger correction, as for the older systems.

Resolution and PVE are to be corrected using calibration factors calculated from images of cylinders of various sizes. Calibration factors were produced from images of 6 cylinders scanned together in one image in one phantom. This was appropriate because patients in the pilot study tended to have multiple lesions at sites throughout the body (Ho *et al* 2013). The effects of imaging the cylinders together on spatial resolution and spill-in of counts will be therefore replicated (Mustafovic 2001).

A further challenge to quantitative imaging was that the manufacturers' reconstruction platforms tended to add scaling factors at reconstruction that were difficult to identify. Therefore all trial data were reconstructed centrally using HERMES Hybrid Recon reconstruction software to avoid this complication. This software can reconstruct raw data from all the different manufacturers' SPECT/CT systems in a reproducible way.

The reconstruction parameters were chosen in the first instance to provide and image on which the patients lesions were adequately identifiable for VOI definition.

Triple energy windows were acquired to allow assessment of TEWC scatter correction in the future. However it has been shown that a geometry dependent weighting factor, varying from 0.25 to 0.63, of the TEWC scatter estimate is required (van Gils *et al* 2016). Additionally count rate specific calibration factors are required for use with TEWC, because the energy spectrum varies with count rate due to pulse pile-up (Schipper *et al* 2012). Monte Carlo based correction methods negate these issues. Therefore Monte Carlo scatter correction on the HERMES Hybrid Recon reconstruction platform was implemented for the initial calibrations. Resolution recovery methods, for example through detector collimator response modelling, were not used due to the image artefacts that lead to increased counts at the edge of objects (Kangasmaa *et al* 2011). The effect of the choice of reconstruction parameters, reconstruction platform, compensation methods (such as TEWC) and out-of-FOV activity is to be investigated further.

Calibration factors created for the Hermes Hybrid reconstruction with 32 equivalent OSEM iterations varied between the eight centres, particularly between the two manufacturers. Therefore a standardised calibration process across all centres is currently needed to ensure accurate image quantification for dosimetry. However the factors were similar between the manufacturers' systems, so comparison to other similar systems validated the factors and ensured that the SPECT/CT systems were set up correctly for quantitative imaging.

A similar system response is to be expected for systems of the same make, model and crystal thickness given that SPECT/CT systems are tested at acceptance to be within tolerance of the specification supplied by the manufacturers for each model (NEMA 2007). Therefore validation measurements were made for one of each of the manufacturers systems.

In order to demonstrate the limits of the accuracy of this calibration method a 3D-printed phantom was created to simulate the challenge of patient imaging. The lesion-shaped inserts of this phantom tested the consequence of using calibration factors from cylindrical phantoms for this different geometry. Uncertainty propagation of the calibrator accuracy, system sensitivity reproducibility and the limits on VOI placement accuracy due to the SPECT image spatial resolution were used to calculate the limits on the accuracy of this quantitative imaging method (Gear *et al* 2018). These inaccuracies varied with the object volume and were 10% and 16% on average for ^{123}I and ^{131}I respectively for the 5 cm sphere, demonstrated in table 6. Therefore the uncertainty on the sphere activity in the ^{123}I image would be lower than in the ^{131}I image. The main factors contributing to this difference are the sensitivity uncertainty and the count inaccuracy due to the VOI placement. These influences are larger for ^{131}I than ^{123}I. The larger variation in count sensitivity with geometry for ^{131}I is likely to be due to the increased septal penetration for ^{131}I imaging. The medium energy collimators block the majority of photons penetrating the septa from ^{123}I. The system sensitivity will also depend on the scatter and AC accuracies which will vary with geometry. The dead time correction factor will also vary with the imaged objects geometry, which for this torso-shaped phantom, with active inserts and varied attenuation factors was very different to the uniformly filled cylinder used for the dead time characterisation. Further investigation of this influence is warranted. The accuracy of the VOI placement on the SPECT image will also depend on the spatial resolution, which is poorer for ^{131}I thereby increasing the associated uncertainty.

The percentage differences, $\%D$, of the SPECT image quantification from the calibrator measurements, were similar to those predicted by the calculated uncertainties, $u(\widetilde{A})$, for the individual lesion-shaped inserts. Therefore this method of inaccuracy determination is as applicable to lesion shapes as it is for the spheres. The average inaccuracies in the SPECT/CT images were 3.2% higher for ^{131}I than ^{123}I. Respectively 3/12 and 1/12 of the ^{123}I and ^{131}I errors were not covered by the calculated measurement uncertainties. This form of uncertainty estimate, based on the standard errors, is intended to capture 67% of the data. Therefore these uncertainties are a true reflection of the level of accuracy that may be achieved with these imaging methodologies. Continuation of the validation process with the sphere measurements alone would therefore expect the activity concentrations in the images to be measured within 10% and 16% of the true value for ^{123}I and ^{131}I respectively.

In order to perform accurate dosimetry there are many more challenges when applying these factors to patient scans. In particular, VOI delineation will have a large impact on the determination of the calibration and dose factors. Further optimisation of the dosimetry methods, specifically for this trial will be made as patient data becomes available.

Overall it required 1.5 working days to set-up the acquisition protocols and to acquire the calibration data for each SPECT/CT system following this standardised protocol. The radiation doses received by staff performing these measurements were within occupational dose constraints. Therefore it is practical to set-up multiple sites for quantitative radioiodine imaging for dosimetry.

However the calibration factors are sufficiently similar between cameras from the same manufacturer that global calibration curves could be applied to systems of the same make, model and crystal thickness. These factors would be acquisition and reconstruction protocol specific. It is therefore possible for each system to be considered as set up if checks are in place to ensure that the factors are applied correctly. It is recommended that

validation measurements on each system would be performed for at least three object volumes from 10 to 200 ml for each radioisotope. For ^{131}I this would need to be above 1.6 GBq to check that count losses are consistent with those modelled for the system. This would further simplify system calibration to enable quantitative imaging, thereby reducing the costs and burden for centres wishing to participate in MRT trials that incorporate dosimetry.

These methods could be applied to any radioiodine therapy trial with dosimetry based on ^{123}I or ^{131}I imaging. For example the improved dead-time of the modern SPECT/CT systems will be beneficial for acquiring early time points where higher ^{131}I activities are administered, including for example for ^{131}I metaiodobenzylguanidine (mIBG) treatments. The methods developed and employed here could be adapted to establish networks of calibrated centres for multicentre trials involving other radionuclides.

5. Conclusions

This work demonstrates that it is feasible for multiple centres to perform accurate, standardised quantitative radioiodine imaging. This is necessary to obtain reproducible dosimetry results between centres participating in MRT studies involving dosimetry. The modern SPECT/CT systems assessed in this study have demonstrated low dead-time, which will allow patients to be scanned at activities of at least 3 GBq. The set up time for each SPECT/CT system was 1.5 d. Although calibration factors vary between the various makes and models of SPECT/CT systems, demonstrating the current requirement for individual centre calibration, there was sufficient similarity between matched makes and models to allow the use of global model specific calibration factors in the future. Validation of these methods demonstrated the limits on the accuracy of SPECT/CT radioiodine quantification.

Acknowledgments

The SEL-I-METRY trial is supported by a Cancer Research UK Grant (trial number CRUK/14/041). GE has provided a discount for ^{123}I used in the study, including for these calibration measurements. This research was also supported by AstraZeneca and Sanofi Genzyme. MEDIRAD, EC Horizon 2020 NFRP-9 have provided further support and MEDIRAD receives funding from the Euratom research and training programme 2014–2018 under grant agreement No 755523. We acknowledge additional NHS funding to the NIHR Biomedical Research Centre and Clinical Research Facility in Imaging at The Royal Marsden and Institute of Cancer Research and the Radiotherapy Trials Quality Assurance Group.

ORCID iDs

Rebecca A Gregory https://orcid.org/0000-0003-1264-2855
Glenn Flux https://orcid.org/0000-0003-4743-2276

References

2013/59/Euratom C D 2014 Council Directive 2013/59/Euratom of 5 December 2013 laying down basic safety standards for protection against the dangers arising from exposure to ionising radiation, and repealing Directives 89/618/Euratom, 90/641/Euratom and 2003/122/Eutatom *Off. J. Eur. Union* **57** 1–73

Bailey D L and Willowson K P 2014 Quantitative SPECT/CT: SPECT joins PET as a quantitative imaging modality *Eur. J. Nucl. Med. Mol. Imaging* **41** S17–25

Brown S R *et al* 2019 Investigating the potential clinical benefit of Selumetinib in resensitising advanced iodine refractory differentiated thyroid cancer to radioiodine therapy (SEL-I-METRY): protocol for a multicentre UK single arm phase II trial *BMC Cancer* **19** 582

Capintec 2017 *CRC-55t Owner's Manual* (Florham Park, NJ: Capintec Inc.)

Dewaraja Y K *et al* 2013 MIRD pamphlet no. 24: guidelines for quantitative 131I SPECT in dosimetry applications *J. Nucl. Med.* **54** 2182–8

Dietlein M, Eschner W, Grunwald F, Lassmann M, Verburg F A and Luster M 2016 Procedure guidelines for radioiodine therapy of differentiated thyroid cancer. Version 4 *Nuklearmedizin. Nucl. Med.* **55** 77–89

Flux G D, Haq M, Chittenden S J, Buckley S, Hindorf C, Newbold K and Harmer C L 2010 A dose-effect correlation for radioiodine ablation in differentiated thyroid cancer *Eur. J. Nucl. Med. Mol. Imaging* **37** 270–5

Gadd R, Baker M, Nijran K S, Owens S, Thomson W, Woods M J and Zananiri F 2007 Protocol for establishing and maintaining the calibration of medical radionuclide calibrators and their quality control National Physical Laboratory Measurement Good Practice Guide no. 93

Gear J I, Cox M G, Gustafsson J, Gleisner K S, Murray I, Glatting G, Konijnenberg M and Flux G D 2018 EANM practical guidance on uncertainty analysis for molecular radiotherapy absorbed dose calculations *Eur. J. Nucl. Med. Mol. Imaging* **45** 2456–74

Gear J I, Long C, Rushforth D, Chittenden S J, Cummings C and Flux G D 2014 Development of patient-specific molecular imaging phantoms using a 3D printer *Med. Phys.* **41** 082502

Giammarile F, Chiti A, Lassmann M, Brans B and Flux G 2018 EANM procedure guidelines for ^{131}I-meta-iodobenzylguanidine (^{131}I-mIBG) therapy *Eur. J. Nucl. Med. Mol. Imaging* **35** 1039–47

Green P 1990 Bayesian reconstructions from emission tomography data using a modified EM algorithm *IEEE Trans. Med. Imaging* **9** 84–93

Gregory R A, Murray I, Gear J, Aldridge M D, Levine D, Fowkes L, Waddington W A, Chua S and Flux G 2017 Objective comparison of lesion detectability in low and medium-energy collimator iodine-123 mIBG images using a channelized Hotelling observer *Phys. Med. Biol.* **62** 17–30

Ho A L *et al* 2013 Selumetinib-enhanced radioiodine uptake in advanced thyroid cancer *New Engl. J. Med.* **368** 623–32

Hoffman E J, Huang S C and Phelps M E 1979 Quantitation in positron emission computed tomography: 1. Effect of object size *J. Comput. Assist. Tomogr.* **3** 299–308

Inoue Y, Ohtake T, Yoshikawa K, Nishikawa J and Sasaki Y 1998 Estimation of deadtime in imaging human subjects *Eur. J. Nucl. Med.* **25** 1232–7

Kangasmaa T, Sohlberg A and Kuikka J T 2011 Reduction of collimator correction artefacts with Bayesian reconstruction in spect *Int. J. Mol. Imaging* **2011** 6

Luster M, Clarke S E, Dietlein M, Lassmann M, Lind P, Oyen W J, Tennvall J and Bombardieri E 2008 Guidelines for radioiodine therapy of differentiated thyroid cancer *Eur. J. Nucl. Med. Mol. Imaging* **35** 1941–59

Madsen M T and Nickles R J 1986 A precise method for correcting count-rate losses in scintillation cameras *Med. Phys.* **13** 344–9

Maxon H R, Thomas S R, Hertzberg V S, Kereiakes J G, Chen I W, Sperling M I and Saenger E L 1983 Relation between effective radiation dose and outcome of radioiodine therapy for thyroid cancer *N. Engl. J. Med.* **309** 937–41

Maxon H R III, Englaro E E, Thomas S R, Hertzberg V S, Hinnefeld J D, Chen L S, Smith H, Cummings D and Aden M D 1992 Radioiodine-131 therapy for well-differentiated thyroid cancer—a quantitative radiation dosimetric approach: outcome and validation in 85 patients *J. Nucl. Med.* **33** 1132–6

McGowan D R and Guy M J 2015 Time to demand dosimetry for molecular radiotherapy? *Br. J. Radiol.* **88** 20140720

Mustafovic K T, Hogg D and Bloomfield P 2001 Object dependency of resolution and convergence rate in OSEM with filtering *IEEE Nuclear Science Symp. Medical Imaging Conf. Record* pp 1786–90

National Cancer Research Institute 2016 *CTRad: Identifying Opportunities to Promote Progress in Molecular Radiotherapy Research in the UK* (National Cancer Research Institute (London: NCRI))

National Electrical Manufacturers Association 2007 Performance measurements of gamma cameras NEMA Standards Publication NU 1- 2007 (Rosslyn, VA: NEMA)

Rosenthal M S, Cullom J, Hawkins W, Moore S C, Tsui B M and Yester M 1995 Quantitative SPECT imaging: a review and recommendations by the Focus Committee of the Society of Nuclear Medicine Computer and Instrumentation Council *J. Nucl. Med.* **36** 1489–513

Schipper M J, Koral K F, Avram A M, Kaminski M S and Dewaraja Y K 2012 Prediction of therapy tumor-absorbed dose estimates in I-131 radioimmunotherapy using tracer data via a mixed-model fit to time activity *Cancer Biother. Radiopharm.* **27** 403–11

Silberstein E B *et al* 2012 The SNMMI practice guideline for therapy of thyroid disease with ^{131}I 3.0 *J. Nucl. Med.* **53** 1633–51

Silosky M, Johnson V, Beasley C and Kappadath S C 2013 Characterization of the count rate performance of modern gamma cameras *Med. Phys.* **40** 032502

Siman W, Silosky M and Kappadath S C 2015 A revised monitor source method for practical deadtime count loss compensation in clinical planar and SPECT studies *Phys. Med. Biol.* **60** 1199–216

Sohlberg A O and Kajaste M T 2012 Fast Monte Carlo-simulator with full collimator and detector response modelling for SPECT *Ann. Nucl. Med.* **26** 92–8

Sorenson J A 1975 Deadtime characteristics of anger cameras *J. Nucl. Med.* **16** 284–8

van Gils C A, Beijst C, van Rooij R and de Jong H W 2016 Impact of reconstruction parameters on quantitative I-131 SPECT *Phys. Med. Biol.* **61** 5166–82

Wadsley J, Gregory R, Flux G, Newbold K, Du Y, Moss L, Hall A, Flanagan L and Brown S R 2017 SELIMETRY-A multicentre I-131 dosimetry trial: a clinical perspective *Br. J. Radiol.* **90** 20160637

Wierts R, Brans B, Havekes B, Kemerink G J, Halders S G, Schaper N N, Backes W H, Mottaghy F M and Jentzen W 2016 Dose-response relationship in differentiated thyroid cancer patients undergoing radioiodine treatment assessed by means of ^{124}I PET/CT *J. Nucl. Med.* **57** 1027–32

Zimmerman B E *et al* 2017 Multi-centre evaluation of accuracy and reproducibility of planar and SPECT image quantification: an IAEA phantom study *Z. Med. Phys.* **27** 98–112